American Journal of BioMedicine
AJBM 2022;10 (2): 35-48
Research Article doi:10.18081/2333-5106/2022.10/35

Sequencing of RNAs involved in sepsis-induced myocardial injury: role of Local sympathetic denervation

Puerto D. Alcantara [1], Garcia S. Armada [1], Ryon A. Seldon [1], Christopher C. Burke *[2]

Abstract

Sepsis has been a serious public health concern for a long time and is characterized by disrupted development of specific diagnostic criteria and novel therapies for sepsis is critically dependent on an understanding of the basic mechanisms immune homeostasis accompanied by infection and multiple organ dysfunction as determined assessed by the Sequential Organ Failure. Adult (4 to 6 months) male C57BL/6 mice, animal set in three groups, control group, Cecal Ligation and Puncture (CLP) group, CLP+ Local sympathetic denervation group 8 mice in each group. CLP model for created sepsis and local sympathetic denervation procedure for alleviated the effects of sepsis. Assessment of cardiac function by Millar Instruments, immunofluorescence staining, enzyme-linked immunosorbent assay (ELISA) and RNA extraction and sequencing. Our findings showed that the myocardial injury score and TNF-α level in both tissue and serum were significantly increased in the CLP group. CLP with local sympathetic denervation group mice had lower scores of myocardial injuries. Sepsis augments MCP-1 and KC level in myocardium. After 48 hours after CLP, the myocardial injury score. CLP with local sympathetic denervation alleviates sepsis-induced myocardial injury by inhibiting the NF-κB signaling pathway. Moreover, compared with the Ctrl group, the CLP with local sympathetic denervation group obtained fewer ncRNAs and mRNAs. Inconclusions, the NF-κB signaling pathway is associated with sepsis-induced myocardial injury, and local sympathetic denervation can relieve sepsis-induced myocardial injury by regulating the ncRNAs and mRNAs.

Keywords: RNA; Local sympathetic denervation; sepsis; NF-κB signaling.

*Corresponding author email: cc Burke@hmhospitales.com
[1] Biomédica en Red Enfermedades Respiratorias, Madrid, Spain.
[2] Faculty of Medicine, Sweden.
Received January 22, 2022; revised March 29, 2022; accepted April 09, 2022; published April 15, 2022.

Introduction

As the main cause of death in intensive care units, sepsis has been a serious public health concern for a long time and is characterized by disrupted development of specific diagnostic criteria and novel therapies for sepsis is critically dependent on an understanding of the basic mechanisms immune homeostasis accompanied by infection and multiple organ dysfunction as determined assessed by the Sequential Organ Failure [1]. The of the disease. Numerous

Research Article doi:10.18081/2333-5106/2022.10/25

lines of evidence have concluded that many signaling pathways and pathological processes are involved in sepsis, such as the host immune response, unstable circulation, endothelial barrier dysfunction, and disordered cell function [2, 3].

Myocardial injury is a major and serious complication of sepsis; sepsis-induced myocardial injury has a high incidence rate and is observed in 40–50% of patients with sepsis [4]. Moreover, studies have reported that sepsis-induced cardiac dysfunction may be as high as 70% and is a major predictor of mortality from sepsis [5, 6]. However, current treatments for myocardial injury following sepsis are not ideal, as mechanisms underpinning sepsis-induced myocardial injury are not fully understood.

Sepsis depresses cardiac function via upregulation of the expression of cardiodepressant cytokines, including TNF-α, IL-1β and IL-6 [7]. IL-6 expression is elevated in several tissues of old mice [8]. In addition, aging has been shown to exacerbate the cytokine response to pro-inflammatory insults, including endotoxin, trauma, and ischemia/reperfusion injury [9]. Thus, it is likely that aging upregulates the myocardial inflammatory responses to endotoxin and exaggerates sepsis cardiac depression [10] and the mononuclear cells are major sources of tissue pro-inflammatory cytokines [11].

The sympathetic nervous system has a wide variety of cardiovascular actions, including heart rate acceleration, increase in cardiac contractility, reduction of venous capacitance, and constriction of resistance vessels. On the contrary, the parasympathetic nervous system affects the cardiovascular system by slowing heart rate through vagal impulses [12]. The cardiac sympathetic nerve fibers are located subepicardially and travel along the major coronary arteries representing the predominant autonomic component in the ventricles [13]. The parasympathetic fibers run with the vagus nerve subendocardially after it crosses the atrioventricular groove and are mainly present in the atrial myocardium and less abundantly in the ventricular myocardium [14].

The ventricular sympathetic innervation is characterized by a gradient from base to apex (3). The cardiac neuronal system is made up of spatially distributed cell stations comprising afferent, efferent, and interconnecting neurons behaving as a control system [15]. The neurons are in constant communication with each other, and each neuronal cell station is involved in cardio-cardiac reflexes that control spatially organized cardiac regions [16].

Cardiac sympathetic neuronal activity or its pharmaceutical inhibition can also be noninvasively assessed by the use of ^{123}I-metaiodobenzylguanidine (MIBG), an analogue of NE [17], using semiquantitative analyses, namely early heart-to-mediastinum ratio, late heart-to-mediastinum ratio, and myocardial washout. Beta-blockade and renin-angiotensin-aldosterone inhibition are associated with an increase in ^{123}I-MIBG uptake and a reduced washout. Data from a systematic meta-analysis suggest that patients with decreased late heart-to-mediastinum or increased myocardial ^{123}I-MIBG washout have a worse prognosis than those patients with normal semiquantitative myocardial MIBG parameters [18].

Research Article doi:10.18081/2333-5106/2022.10/25

A prospective study that compared the predictive value of cardiac ^{123}I-MIBG imaging for sudden cardiac death with that of the signal-averaged electrocardiogram, heart rate variability, and QT dispersion in patients with mild-to-moderate heart failure demonstrated that ^{123}I-MIBG was the only powerful predictor of sudden cardiac death independently of left ventricular ejection fraction [19].

Materials and methods

Animals and treatment

Adult (4 to 6 months) male C57BL/6 mice were obtained from the Jackson Laboratory (Bar Harbor, Maine, USA) and National Institute on Aging (Bethesda, MD, USA). Mice were acclimated for 14 days in a 12:12-h light-dark cycle with free access to water and regular chow diet before the experiments. The experiments were approved by the Institutional Animal Care and Use Committee of the Biomédica en Red Enfermedades Respiratorias, and this investigation conforms to the Guide for the Care and Use of Laboratory Animals (National Research Council, revised 1996). Animal set in three groups, control group, Cecal Ligation and Puncture (CLP) group, CLP+ Local sympathetic denervation group 8 mice in each group.

Cecal Ligation and Puncture (CLP) model

It was performed as described previously [20], in briefly anesthetize the mouse by injecting intraperitoneally a solution of 1:1 ketamine (75mg/kg) and xylazine (15mg/kg). As a reference, inject 30 µl of the 1:1 solution into a mouse weighing 20 grams [20]. The cecum is tightly ligated with a 6.0 silk suture (6-0 PROLENE, 8680G; Ethicon) at its base below the ileo-cecal valve and is perforated once or twice with a 19-gauge needle (4 and 5) on the same side of the cecum. Please note that the length of ligated cecum defined as the distance from the distal end of cecum to ligation point will determine the degree of severity. A distance of >1cm produces high grade sepsis while a distance of ≤1 cm produces mid-to-low grade sepsis. The cecum is then gently squeezed to extrude a small amount of feces from the perforation sites. The cecum is returned to the peritoneal cavity and the peritoneum is closed with 6.0 silk sutures.

The skin is closed with Reflex 7mm clips (RS-9258, Roboz Surgical Instruments) or Michel wound clips (7 mm, RS-9270). Resuscitate mice by injecting subcutaneously 1 ml of pre-warmed 0.9% saline solution using a 25G needle. This fluid resuscitation measure will induce the hyperdynamic phase of sepsis. Mice of sham as control group only received cecum exposure without ligation or puncture. All mice were resuscitated by sterile 0.9% saline at the end of the surgery and had free access to water and food.

Mice were euthanized at 72 hrs after surgery. Tissues of lungs, heart, liver and kidney were harvested and fixed in 4% paraformaldehyde at 4°C or stored at −80°C immediately. Whole blood was centrifuged at 3000 rpm for 15 mins and sera were collected and stored at −80°C. After analysis of cardiac function, the heart tissue and blood were collected and prepared for analysis.

Local sympathetic denervation

It was performed as described previously for rats [21], briefly after induction of anesthesia, a vertical neck incision (~10 mm) was made and kept open using placeholders. Next, the salivary glands were carefully dissected from the caudal adhesive tissue and flipped aside. The position was then corrected by adjusting the lower two placeholders (with expanded surface). With blunt forceps, the sternocleidomastoid muscle was lifted, moved aside, and held using the upper two, thinner placeholders. Lateral positioning of the sternocleidomastoid muscle allowed for clear visibility of the carotid artery. The common carotid artery (CCA) was followed in cranial direction to locate the carotid bifurcation (in internal and external carotid arteries). The almond-shaped superior cervical ganglia (SCG) are located behind the carotid bifurcation.

This approach exposed the preganglionic and postganglionic branches of the SCG, facilitating complete removal of the ganglion itself. The ganglionic cell body was fully extracted by shifting the external carotid artery to the lateral side using a special 90° angled forceps. Finally, the SCG was detached from the sympathetic chain and the SCG tissue was collected. Complete cardiac sympathetic denervation was achieved by additional removal of the SCG on the contralateral side.

Measurement of cardiac function

We assessed cardiac function at 48 h after CLP as described previously [22]. Briefly, mice were anesthetized with pentobarbital sodium (Vortech Pharmaceuticals, Dearborn, MI, USA; 50 mg/kg, intraperitoneal (ip)) and anticoagulated with heparin (Elkins-Sinn, Cherry Hill, NJ, USA; 1,000 units/kg, ip). Animals were laid supine on a heating blanket and core body temperature was maintained at 37°C ± 0.5°C. A microcatheter (Millar Instruments, Houston, TX, USA; 1 F) was inserted into the left ventricle (LV) through the right common carotid artery. Pressure-volume loop was recorded using the MPVS-400 system with the aid of PVAN software (Millar Instruments). Heart rates, LV pressure, LV volume, and related function parameters were analyzed: 10 μL of 30% saline was injected into the inferior vena cava for actual ventricle volume calculation.

Immunofluorescence staining

The optimal cutting temperature (OCT)-embedded tissues were cut into thin sections (5-μm thick). Sections were treated with a mixture of 30% acetone and 70% methanol for 5 minutes, washed with PBS and fixed with 4% paraformaldehyde. Then sections were incubated with a rabbit polyclonal antibody against murine CD68 (a marker of mononuclear cells, including monocytes and macrophages) followed by Cy3-tagged goat anti-rabbit IgG (imaged on the red channel). Nuclei were stained with bis-benzimide (4′,6-diamidino-2-phenylindole (DAPI), imaged on the blue channel), and glycoproteins on cell surfaces were stained with Alexa 488-tagged wheat germ agglutinin (imaged on the green channel). Microscopy was performed with a Leica DMRXA digital microscope (Leica Mikroskopie and System GmbH, Wetzlar, Germany). Images were analyzed in a blinded fashion.

Research Article doi:10.18081/2333-5106/2022.10/25

Enzyme-linked immunosorbent assay (ELISA)

Commercial ELISA kits (R & D Systems) were utilized to quantify chemokines (MCP-1, KC and macrophage inflammatory protein-1α (MIP-1α)) and cytokines (TNF-α, IL-1β and IL-6) in plasma and myocardial tissue homogenates, as well as cardiac troponin-I (cTn-I) in plasma. Samples and standards were prepared according to manufacturer's instructions. Absorbance of standards and samples were determined spectrophotometrically at 450 nm, using a microplate reader (Bio-Rad Laboratories, Inc, Hercules, CA, USA). Results were plotted against the linear portion of a standard curve.

RNA extraction and sequencing

The mice (n = 8) in each group were anesthetized, and cardiac tissues were quickly transferred to liquid nitrogen and transported to the sequencing laboratory with dry ice. The mirVana™ miRNA Isolation Kit and Ambion-1561 were used to extract total RNA, after which TruSeq Stranded Total RNA with Ribo-Zero Gold was used for library construction. Generally, the RNA was broken into short fragments. The first and second cDNA strands were synthesized in turn. dTTP was replaced with dUTP in the second cDNA strand after end repair, ligation of the sequencing adapters and digestion by the UNG enzyme. PCR amplification was then performed. After quality inspection, an Illumina sequencer was used for sequencing, and clean reads were obtained for subsequent analysis.

Briefly, the RseQC(2.6.4), fastqc(v0.11.5), HISAT2(2.2.1.0), and Stringtie2(1.3.3b) software programs were used for quality control, genome alignment and transcript splicing. The circRNAs were predicted using CIRI (v2.0.3) software [23]. Finally, the DE circRNAs, DE lncRNAs, and DE mRNAs were analyzed with DESeq2 (1.18.0) software.

Quantification of miRNAs and identification of DE miRNAs

After total RNA was extracted from the samples, a miRNA sequencing library was constructed using the mirVana miRNA Isolation Kit (Ambion) and TruSeq Small RNA Sample Prep Kits. Total RNA, concentration and integrity were measured by Nanodrop 2000 and Agilent 2100. After PCR amplification and quality inspection, the library was sequenced using an Illumina HiSeq X Ten platform. High-quality clean reads were obtained after filtering using Fastx-toolkit (0.0.13) software, Bowtie (1.1.1) and NGSQCToolkit.

The clean reads were aligned to the mouse genome and compared with miRBase (version 22.0). Target genes of DE miRNAs were predicted by Miranda (3.3a). The expression levels of the identified known mature miRNA sequences and the newly predicted miRNAs were quantified as the transcripts per million (TPM). DE miRNAs were analyzed with DESeq2 (1.18.0) software.

Research Article doi:10.18081/2333-5106/2022.10/25

Statistical methods

Data are presented as mean ± standard error (SE). Statistical analysis was performed using StatView software (Abacus Concepts, Calabasas, CA, USA). Analysis of variance (ANOVA) with Fisher post-hoc test was used to analyze differences between experimental groups, and differences were confirmed using the Mann-Whitney *U*-test. Statistical significance was defined as $P \leq 0.05$.

Results

In septic rats, myocardial contraction and diastolic function were weakened, which often manifested as heart failure, impaired myocardial function, increased mortality, and increased inflammatory factors. The representative pressure-volume loops in Figure 1, sepsis causes a reduction in LV function, and old mice have worse LV function during sepsis.

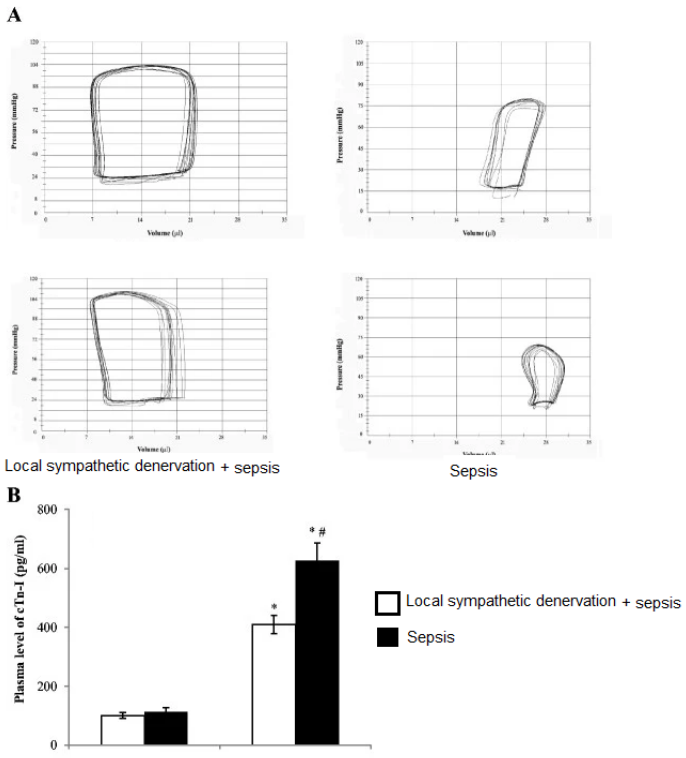

Figure 1.

Sepsis results in greater cardiac depression and worse myocardial injury in old mice.

Adult mice were suspected to CLP. Left ventricular pressure-volume loops and plasma levels cardiac troponin-I (cTn-I) were analyzed 48 days after CLP. Sepsis mice displayed greater reduction in left ventricular performance (A) and higher levels of cTn-I in plasma (B). Data are expressed as mean ± standard error; *P <0.05 versus corresponding local sympathetic denervation; #P <0.05 versus adult mice with sepsis only.

Research Article doi:10.18081/2333-5106/2022.10/25

Sepsis results in attenuated cardiac function

We determined whether sepsis causes attenuated cardiac function in CLP mice than in local sympathetic denervation. Heart rate increased in both CLP mice and local sympathetic denervation in comparison to saline-treated controls (Table 1). Compared to the control group, ejection fraction and developed pressure decreased in CLP mice more than local sympathetic denervation. Similarly, cardiac output was decreased in CLP mice and improved in local sympathetic denervation.

Table 1.

Left ventricle function parameters.

Parameter	Control	CLP	CLP +sympathetic denervation
Heart rate (bpm)	460 ± 11	480 ± 21*	455 ± 10*
Developed pressure (mmHg)	89.0 ± 3.0	50.0 ± 1.0*	68.1 ± 2.0*†
End-systolic volume (μL)	8.0 ± 1.3	19.4 ± 1.0*	12.5 ± 1.2*†
End-diastolic volume (μL)	22.0 ± 1.3	29.0 ± 1.4*	26.1 ± 1.1*
Ejection fraction (%)	69.1 ± 2.2	30.3 ± 1.8*	46.1 ± 1.2*†
Cardiac output (mL/min)	6.2 ± 0.2	3.1 ± 0.2*	4.9 ± 0.2*†

Sepsis augments MCP-1 and KC level in myocardium

Sepsis increased the levels of MCP-1 and KC in plasma and the myocardium (Figure 2A and B). Interestingly, local sympathetic denervation (LSD) mice had significantly higher levels of MCP-1 and KC in plasma and the myocardium than CLP mice only.

Research Article doi:10.18081/2333-5106/2022.10/25

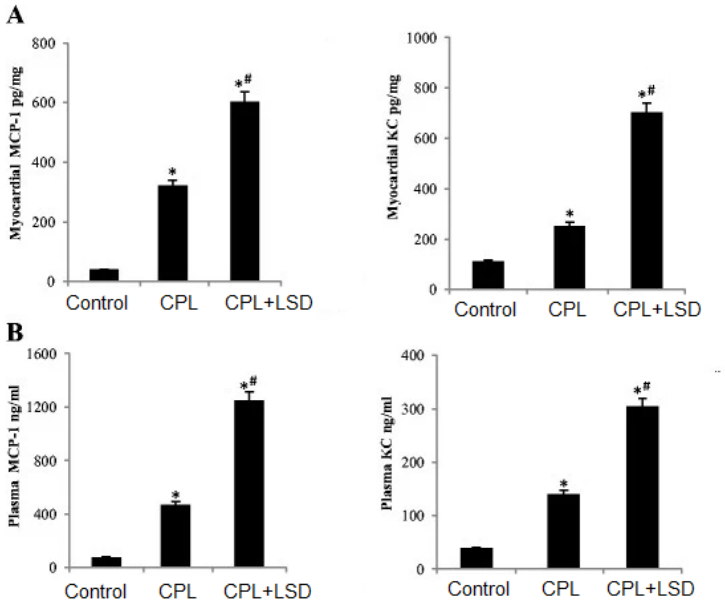

Figure 2.

CLP mice have higher levels of chemokines in the myocardium and plasma.

Levels of MCP-1 and KC were analyzed by ELISA 48 h after CLP. CLP mice only had higher levels of MCP-1 and KC in myocardial tissue (A) and plasma (B). Data are expressed as mean ± standard error. *P <0.05 versus corresponding control (Ctrl); #P <0.05 versus CLP only mice.

CLP with local sympathetic denervation alleviates sepsis-induced myocardial injury by inhibiting the NF-κB signaling pathway

There was no significant difference in the myocardial injury score of heart tissue between the Ctrl group and CLP with local sympathetic denervation group (Fig. 3a, b). After CLP, the myocardial injury score and TNF-α level in both tissue and serum were significantly increased in the CLP group. CLP with local sympathetic denervation group mice had lower scores of myocardial injuries.

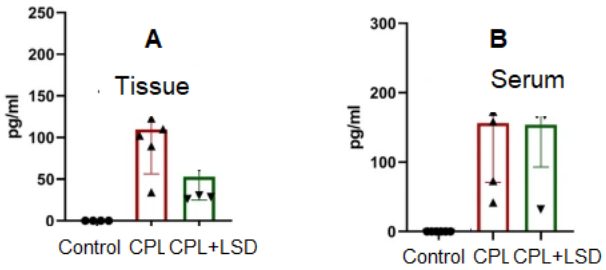

Figure 3.

Local sympathetic denervation alleviated. A/ TNF-α levels in tissue. B/ TNF-α levels in serum. Data represent the mean ± sd. *p < 0.05.

Research Article doi:10.18081/2333-5106/2022.10/25

RT-qPCR verification of DE miRNAs and DE circRNAs

The results of RT-qPCR confirmed the DE miRNAs and DE circRNAs identified by sequencing. The expression levels of miRNA-133b-3p (Fig. 4a) and miR-486b-3p (Fig. 4b) were significantly lower in the CLP group than in the Ctrl group. In comparison, the expression levels of miRNA-133b-3p (Fig. 4a), miR-486b-3p (Fig. 4b) and miRNA-135b-5p (Fig. 4c) were significantly higher in the CLP with local sympathetic denervation group mice than in the CLP group. The expression levels of circRNA-0000246 (Fig. 4d), circRNA-003646 (Fig. 4e), and circRNA-0013022(Fig. 4f) were consistent with the sequencing results.

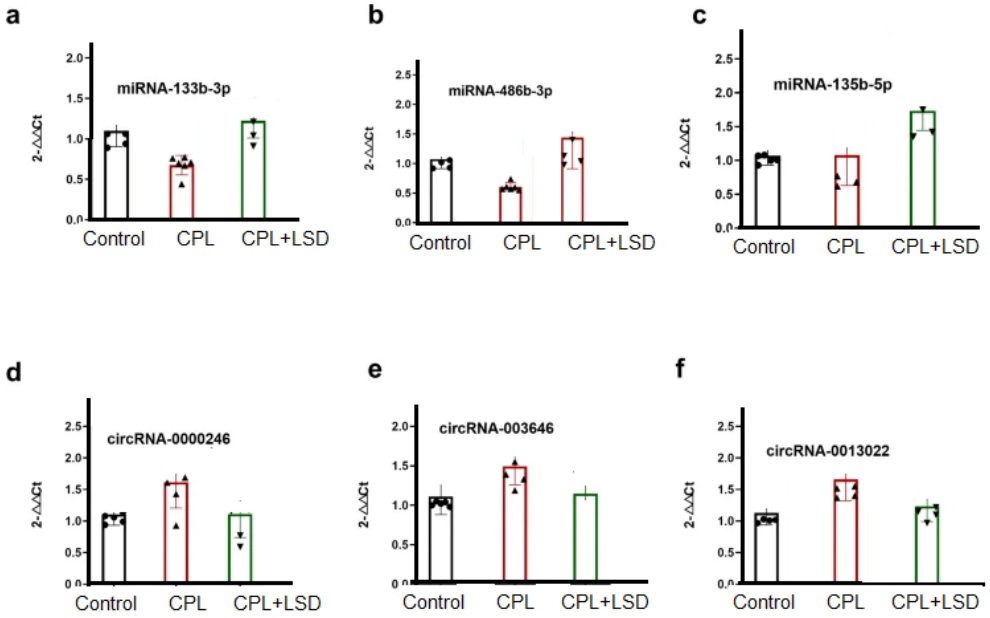

Figure 4.

DE circRNA, lncRNAs, miRNAs, and mRNAs

Compared with the Ctrl group, the CLP with local sympathetic denervation group obtained fewer ncRNAs and mRNAs (Figs. 4, 5a, 5d, 6a, 6d, 7a, 7d, S2a, S2d), while compared with the Ctrl group, the ALI group exhibited 668 DE circRNAs, of which 304 were upregulated and 364 were downregulated (Figs. 4a, 5b, 5e); 814 DE lncRNAs, of which 511 were upregulated and 303 were downregulated (Figs. 4b, 6b, 6e); 22 DE miRNAs, of which 14 were upregulated and 8 were downregulated (Figs. 4c, 7b, 7e); and 1598 DE mRNAs were identified, of which 1144 were upregulated and 454 were downregulated(Fig. 4d, S2b, S2e).

Discussion

The immune and the nervous systems intensely interact and mutually control each other [24]. In peripheral tissues, the sympathetic nervous system has been demonstrated to regulate key processes of immune cell function, such as the release of monocytes from the bone marrow compartment [25] tissue programming of macrophages [27], the cytokine expression profile of various immune cells [28], and the antibody production of B cells [29].

Research Article doi:10.18081/2333-5106/2022.10/25

A detailed picture of the signalling pathways and molecules involved that execute these diverse functions is only gradually evolving. Upon their activation, postganglionic sympathetic fibers release norepinephrine together with several cotransmitters (e.g., adenosine triphosphate). Norepinephrine exerts its function on recipient cells through the binding and activation of adrenoceptors, among which the beta-2-adrenoceptor and the beta-3-adrenoceptor have been assigned critical roles in regulating immune cell function or their mobilization [30].

Sepsis causes whole body dysfunction due to infection and is one of the leading causes of mortality worldwide [31]. While it has been studied for ~2,000 years, the incidence of sepsis has not decreased over time [32]. Inflammation is the first characteristic feature of sepsis. Previous studies have revealed that oxidative stress caused by inherent inflammatory responses can lead to the initiation of lipid peroxidation, DNA damage and mitochondrial function deterioration, as well as further the development of organ dysfunction and failure [33]. Therefore, increases in inflammation and oxidative stress both contribute to the damage caused by sepsis [30].

Moreover, oxidative stress has been reported to participate in numerous pathological conditions, such as diabetes and myocardial ischemia reperfusion injury [33].

NcRNAs play essential roles in myocardial injury and many other systems such as lung tissue. To further explore the mechanism of sympathetic nerve regulation in myocardial injury, we investigated whether sympathetic nerves affect circRNA, lncRNA, or miRNA levels during sepsis-induced myocardial injury. We found many differentially expressed circRNAs, lncRNAs, miRNAs, and mRNAs in the CLP group, compared with the Ctrl group that regulated inflammatory signaling pathways indicated by GO and KEGG enrichment. Some previous studies have also used whole-transcriptome sequencing to assess the transcriptome changes in myocardial injury and have proven that multiple circRNAs, lncRNAs, miRNAs, and mRNAs are significantly altered in myocardial injury [34].

In the current study, we identified 629 DE circRNAs, 269 DE lncRNAs, 192 DE mRNAs, and 7 DE circRNAs in the CLP with local sympathetic denervation group compared with the CLP group. We performed GO and KEGG enrichment analyses to further understand the roles of these DE ncRNA and DE mRNAs. GO and KEGG enrichment analyses of the DE ncRNAs and DE mRNAs in the CLP group showed that many immune-inflammatory processes and pathways included the NF-κB signaling pathway. Surprisingly, many DE circRNAs, DE lncRNAs, DE miRNAs, and DE mRNAs were found in the CLP with local sympathetic denervation group compared with the CLP group, too. GO and KEGG analyses identified many inflammatory and immune responses such as the TGF-β signaling pathway, TNF signaling, MAPK signaling, Th17 cell differentiation, and B-cell receptor signaling pathways, between the DE ncRNAs and the DE mRNAs.

Research Article doi:10.18081/2333-5106/2022.10/25

Conclusion

NF-κB signaling pathway is associated with sepsis-induced myocardial injury, and local sympathetic denervation can relieve sepsis-induced myocardial injury by regulating the ncRNAs and mRNAs.

Competing interests

The authors declare no conflict of interest.

Ethics approval and consent to participate

This study was approved by the Institutional Ethics Committee of: The Medical Committee of Biomédica en Red Enfermedades Respiratorias.

Authors' contributions

All authors shared in the conception and design and interpretation of data, drafting of the manuscript and critical revision of the case study for intellectual content and final approval of the version to be published. All authors read and approved the final manuscript.

Open access

References

1. Lymperopoulos A, Rengo G, Koch WJ. Adrenergic nervous system in heart failure. Circ Res 2013; 113:739–753.
2. Scheiermann C, Kunisaki Y, Lucas D, et al. Adrenergic nerves govern circadian leukocyte recruitment to tissues. Immunity 2012; 37:290–301.
3. Wang Y, Liu J, Suo F, et al. Metoprolol-mediated amelioration of sympathetic nerve sprouting after myocardial infarction. Cardiology 2013; 126:50–58.
4. Pham T, Rubenfeld GD. Fifty years of research in ARDS. The epidemiology of acute respiratory distress syndrome. A 50th birthday review. Am J Respir Crit Care Med. 2017; 195(7):860–70.
5. Morel E, Mehrpour M, Botti J, Dupont N, Hamai A, Nascimbeni AC, Codogno P. Autophagy: A druggable process. Annu Rev Pharmacol Toxicol. 2017; 57:375–398.
6. Tay Y, Rinn J, Pandolfi PP. The multilayered complexity of ceRNA crosstalk and competition. Nature. 2014; 505(7483):344–52.

7. Abboud FM, Harwani SC, Chapleau MW. Autonomic neural regulation of the immune system: implications for hypertension and cardiovascular disease. Hypertension 2012; 59:755–762.
8. Kim J, Kundu M, Viollet B, Guan KL. AMPK and mTOR regulate autophagy through direct phosphorylation of Ulk1. Nat Cell Biol. 2011; 13:132–141.
9. Kasprowicz DJ, Kohm AP, Berton MT, Chruscinski AJ, Sharpe A, Sanders VM. Stimulation of the B cell receptor, CD86 (B7-2), and the 2-adrenergic receptor intrinsically modulates the level of IgG1 and IgE produced per B cell. J Immunol 2000; 165:680–690.
10. Nishida K, Okinaga K, Miyazawa Y, Suzuki K, et al. Emergency abdominal surgery in patients aged 80 years and older. Surg Today. 2000, 30: 22-27.
11. Zhang M, Wang C, Hu J, et al. Notch3/Akt signaling contributes to OSM-induced protection against cardiac ischemia/reperfusion injury. Apoptosis. 2015; 20:1150–1163.
12. Chen C, He Y, Feng Y, Hong W, Luo G, Ye Z. Long non-coding RNA review and implications in acute lung inflammation. Life Sci. 2021; 269:119044.
13. Jiang Y-H, Jiang P, Yang J-L, et al. Cardiac dysregulation and myocardial injury in a 6-hydroxydopamine-induced rat model of sympathetic denervation. PLoS One 2015; 10:1–19.
14. Nagatsu T, Nagatsu I. Tyrosine hydroxylase (TH), its cofactor tetrahydrobiopterin (BH4), other catecholamine-related enzymes, and their human genes in relation to the drug and gene therapies of Parkinson's disease (PD): historical overview and future prospects. J Neural Transm 2016; 123:1255–1278.
15. Ram R, Mickelsen DM, Theodoropoulos C, Blaxall BC. New approaches in small animal echocardiography: imaging the sounds of silence. Am J Physiol Heart Circ Physiol 2011; 301:H1765–H1780.
16. Tu G, Zou L, Liu S, et al. Long noncoding NONRATT021972 siRNA normalized abnormal sympathetic activity mediated by the upregulation of P2X7 receptor in superior cervical ganglia after myocardial ischemia. Purinergic Signal. 2016; 12(3):521–35.
17. Shen MJ, Zipes DP. Role of the autonomic nervous system in modulating cardiac arrhythmias. Circ Res 2014; 114:1004–1021.
18. Wernli G, Hasan W, Bhattacherjee A, Rooijen N, Smith PG. Macrophage depletion suppresses sympathetic hyperinnervation following myocardial infarction. Basic Res Cardiol 2009; 104:681–693.
19. Antonucci E, Fiaccadori E, Donadello K, Taccone FS, Franchi F, Scolletta S. Myocardial depression in sepsis. From pathogenesis to clinical manifestations and treatment. J Crit Care. 2014; 29:500–511.
20. Toscano MG, Ganea D, Gamero AM. Cecal Ligation Puncture Procedure. J Vis Exp. 2011; (51):2860.
21. Peitzman AB, Udekwu AO, Ochoa J, Smith S: Bacterial translocation in trauma patients. J Trauma. 1991; 31:1083-1086.
22. Kaye D, Esler M. Sympathetic neuronal regulation of the heart in aging and heart failure. Cardiovasc Res 2005; 66:256–264.

23. Marques FZ, Eikelis N, Bayles RG, et al. A polymorphism in the norepinephrine transporter gene is associated with affective and cardiovascular disease through a microRNA mechanism. Mol Psychiatry. 2017; 22(1):134–41.
24. Saliminejad K, Khorram Khorshid HR, Soleymani Fard S, Ghaffari SH. An overview of microRNAs: biology, functions, therapeutics, and analysis methods. J Cell Physiol. 2019;234(5):5451–65.
25. Zhao X, Qi H, Zhou J, Xu S, Gao Y. P27 protects cardiomyocytes from sepsis via activation of autophagy and inhibition of apoptosis. Med Sci Monit. 2018; 24:8565–8576.
26. Kalvari I, Argasinska J, Quinones-Olvera N, et al. Rfam 13.0: shifting to a genome-centric resource for non-coding RNA families. Nucleic Acids Res. 2018; 46(D1):D335–42.
27. Zhang L, Han YJ, Zhang X, Wang X, Bao B, Qu W, Liu J. Luteolin reduces obesity-associated insulin resistance in mice by activating AMPKα1 signalling in adipose tissue macrophages. Diabetologia. 2016; 59:2219–2228.
28. Cai W, Li J, Su J. Effects of renal denervation on the expression profile of circular RNA in the serum of patients with resistant hypertension. Hell J Cardiol. 2022; 63:66–74.
29. Zhang L, Gao J, Cui S. miR-21 is involved in norepinephrine-mediated rat granulosa cell apoptosis by targeting SMAD7. J Mol Endocrinol. 2017;58(4):199–210.
30. Kumar A, Haery C, Parrillo JE: Myocardial dysfunction in septic shock. Crit Care Clin. 2000, 16: 251-287.
31. Li X, Yuan Z, Chen J, et al. Microarray analysis reveals the changes of circular RNA expression and molecular mechanism in acute lung injury mouse model. J Cell Biochem. 2019;120(10):16658–67.
32. Akira S, Takeda K, Kaisho T. Toll-like receptors: critical proteins linking innate and acquired immunity. Nat Immunol. 2001; 2:675-680.
33. Hacham M, White RM, Argov S, Segal S, Apte RN: Interleukin-6 and interleukin-10 are expressed in organs of normal young and old mice. Eur Cytokine Netw. 2004; 15:37-46.
34. Pacher P, Nagayama T, Mukhopadhyay P, Batkai S, Kass DA. Measurement of cardiac function using pressure-volume conductance catheter technique in mice and rats. Nat Protoc. 2008, 3: 1422-1434.

American Journal of BioMedicine
AJBM 2022;**10**(1):25-34
Research Article doi:10.18081/2333-5106/2022.10/25

American Journal of BioMedicine
Journal Abbreviation: AJBM
ISSN: 2333-5106 (Online)
DOI: 10.18081/issn.2333-5106
Publisher: BM-Publisher
Email: editor@ajbm.net